Interstitial fluid flow in canaliculi as a mechanical stimulus for cancellous bone remodeling: *in silico* validation

Yoshitaka Kameo[a], Taiji Adachi[b]

a: Department of Mechanical Engineering, Graduate School of Engineering, Osaka Prefecture University
b: Department of Biomechanics, Research Center for Nano Medical Engineering, Institute for Frontier Medical Sciences, Kyoto University

Corresponding author:	Yoshitaka Kameo, Ph.D.
Mailing Address:	Department of Mechanical Engineering
	Graduate School of Engineering
	Osaka Prefecture University
	1-1 Gakuen-cho, Naka-ku, Sakai-shi, Osaka 599-8531, Japan
Telephone:	+81-72-254-9298
Fax:	+81-72-254-9904
E-mail:	kameo@me.osakafu-u.ac.jp

Submitted to Biomechanics and Modeling in Mechanobiology

on May 8, 2013

Abstract

Cancellous bone has a dynamic 3-dimensional architecture of trabeculae, the arrangement of which is continually reorganized via bone remodeling to adapt to the mechanical environment. Osteocytes are currently believed to be the major mechanosensory cells and to regulate osteoclastic bone resorption and osteoblastic bone formation in response to mechanical stimuli. We previously developed a mathematical model of trabecular bone remodeling incorporating the possible mechanisms of cellular mechanosensing and intercellular communication in which we assumed that interstitial fluid flow activates the osteocytes to regulate bone remodeling. While the proposed model has been validated by the simulation of remodeling of a single trabecula, it remains unclear whether it can successfully represent *in silico* the functional adaptation of cancellous bone with its multiple trabeculae. In the present study, we demonstrated the response of cancellous bone morphology to uniaxial or bending loads using a combination of our remodeling model with the voxel finite element method. In this simulation, cancellous bone with randomly arranged trabeculae remodeled to form a well-organized architecture oriented parallel to the direction of loading, in agreement with the previous simulation results and experimental findings. These results suggested that our mathematical model for trabecular bone remodeling enables us to predict the reorganization of cancellous bone architecture from cellular activities. Furthermore, our remodeling model can represent the phenomenological law of bone transformation toward a locally uniform state of stress or strain at the trabecular level.

Keywords

Bone remodeling, Cancellous bone, Interstitial fluid flow, Canaliculus, Mathematical model, Functional adaptation

1. Introduction

Cancellous bone is porous bone composed of strut-like or plate-like trabeculae forming a well-organized 3-dimensional architecture. The arrangement of the trabeculae is continually renewed via bone remodeling to adapt to the mechanical environment, a phenomenon referred to as Wolff's law (Wolff, 1892, 1986). Remodeling of cancellous bone occurs at the trabecular surface by the collaborative cellular activities of bone-resorbing osteoclasts and bone-forming osteoblasts (Parfitt, 1994). Osteocytes, the most abundant cell type in bone tissue, are postulated to orchestrate the metabolic activities of these effector cells (Tatsumi et al., 2007; Nakashima et al., 2011). Osteocytes are considered to be the most likely mechanosensory cells (Cowin et al., 1991; Bonewald and Johnson, 2008; Adachi et al., 2009a, b, c) from an anatomical point of view because they form a complex intercellular network via slender cell processes housed in the porosities, called the lacuno-canalicular system, inside the mineralized bone matrix (Kamioka et al., 2001, 2009; Sugawara et al., 2005).

Although the importance of external forces to the maintenance of bone homeostasis is widely accepted, the mechanism by which the mechanosensory cells transduce these mechanical signals into the biochemical signals for bone remodeling remains unclear. A number of experimental and theoretical studies suggest that dynamic loading-induced flow of the interstitial fluid in the lacuno-canalicular porosities plays a critical role in the excitation of osteocytes (Weinbaum et al., 1994; Knothe Tate et al., 1998; Burger and Klein-Nulend, 1999; Fritton and Weinbaum, 2009). Weinbaum et al. (1994) performed a poroelastic analysis of bone tissue to show that osteocytes can be activated by the fluid-induced shear stress on the

surface membranes of their processes. Subsequent studies identified additional factors that amplify the cellular strain, such as tethering elements connecting the osteocyte processes to the canalicular wall (You et al., 2001; Han et al., 2004) and integrin-mediated focal attachments of the cell processes to the canalicular wall (Wang et al., 2007). More recently, Kamioka et al. (2012) successfully used the technique of ultra-high voltage electron microscopic tomography to reconstruct a 3-dimensional image-based model of a single osteocyte canaliculus for computational fluid dynamics and found that the inhomogeneous flow patterns generated by the highly irregular surface of the canalicular wall may influence osteocytic mechanotransduction.

Computational approaches are essential to the elucidation of the mechanism of bone self-regulation. Computer simulations of bone remodeling enable us to analyze the individual effects of interesting mechanical or biochemical factors in the complex signaling cascade. A variety of mathematical models using finite element analysis has been developed to predict structural changes in bone (Gerhard et al., 2009). The basic concepts of these models are similar; all are based on the common phenomenological hypothesis that bone remodeling is caused by mechanical stimulus at the trabecular level, e.g., strain energy density (SED) (Huiskes et al., 1987, 2000; Mullender et al., 1994; Mullender and Huiskes, 1995; Ruimerman et al., 2005), accumulation of microdamage (Prendergast and Taylor, 1994; McNamara and Prendergast, 2007; Mulvihill and Prendergast, 2008), or local nonuniformity of mechanical quantities such as von Mises equivalent stress (Adachi et al., 1997, 2001; Tsubota et al., 2002, 2009; Tsubota and Adachi, 2004, 2005). While these models provide qualitatively reasonable

results that are consistent with experimental observations, they cannot clarify the relationship between the changes in bone architecture and the mechanical conditions experienced by the osteocytes within the bone matrix.

We previously proposed a mathematical model for trabecular bone remodeling that incorporates the possible mechanisms of cellular mechanosensing and intercellular communication (Adachi et al., 2010; Kameo et al., 2011). In this model, the flow of interstitial fluid inside the canaliculi is explicitly considered to be the mechanical stimulus to osteocytes that regulates bone remodeling. This remodeling simulation can represent the functional adaptation of a single trabecula under physiological cyclic loading. In the present study, we focused on the structural changes in cancellous bone comprising multiple trabeculae to validate our model *in silico* at a more macroscopic level. We combined our remodeling model with the voxel finite element method to demonstrate the changes in cancellous bone morphology in response to uniaxial or bending loads and compared the results with experimental findings and the results of the previous simulation based on the phenomenological law of bone transformation.

2. Methods

2.1. Mathematical model of trabecular bone remodeling

The trabecular bone remodeling is simulated in accordance with the mathematical model previously proposed by the authors (Adachi et al., 2010; Kameo et al., 2011). The theoretical framework is shown in Fig. 1. The mathematical model used here to represent bone cellular

activities in response to mechanical loading is based on the assumption that osteoclastic bone resorption and osteoblastic bone formation are regulated by mechanosensing osteocytes. The process of trabecular bone remodeling is postulated to consist of 3 parts: (i) cellular mechanosensing, (ii) intercellular signal transmission, and (iii) trabecular surface movement due to remodeling. The details of the model are given in Appendix.

2.2. Voxel finite element model of cancellous bone

A 3-dimensional computational model of cancellous bone for simulating the morphological changes in bone tissue caused by local bone remodeling at the trabecular level was constructed as shown in Fig. 2. The region for analysis was $a_1 \times a_2 \times a_3 = 3.2 \times 3.2 \times 3.2$ mm^3 and was divided into $80 \times 80 \times 80$ cubic voxel finite elements with an edge size of 40 μm. This sample size was determined by reference to previous remodeling simulations of cancellous bone (Adachi et al., 2001; Ruimerman et al., 2005). To create an isotropic and uniform porous structure as the starting point for the model of cancellous bone, many pieces of torus-like trabeculae with an outer diameter of 0.36 mm and inner diameter of 0.28 mm were placed randomly throughout the entire region to yield a bone volume fraction BV/TV of 0.4, which is within the physiological range. The effectiveness of this method was proved in 2-dimensional (Tsubota et al., 2002; Jang and Kim, 2008) and 3-dimensional remodeling simulation (Tsubota et al., 2009). The trabecula was modeled as a poroelastic material (Cowin, 1999; Kameo et al., 2008, 2009) with homogeneous and isotropic material properties as listed in Table 1 (Smit et al., 2002; Beno et al., 2006). Two 0.2-mm-thick plates to apply external

load were added to the upper and lower surfaces of the analyzed region. While these plates were given the same material properties as the trabeculae, their shapes were not changed by remodeling.

A shear-free boundary condition was applied to the lower plane, and free leakage of interstitial fluid at the whole trabecular surfaces was assumed. To investigate the effects of different loading patterns on trabecular adaptation, 2 types of monotonously increasing loads $\sigma = \sigma_3(x_1, x_2)t$ were imposed on the upper plane in the x_3 direction for 0.25 sec per day, as shown in Fig. 2. One was (i) a uniaxial load $\sigma_3 = -8$ MPa/sec and the other (ii) a bending load linearly distributed along the x_2 direction from −12 to 12 MPa/sec, i.e., $\sigma_3 = -24x_2/a_2$ [MPa/sec]. The settings of the physiological parameters used in the remodeling model (see Appendix) are summarized in Table 2 (Jaworski and Lok, 1972; You et al., 2004; Huo et al., 2008; Adachi et al., 2009c). All of the parameter settings were based on experimental findings except for 4 parameters associated with the mechanical stimulus, $S_{\mathrm{sf}}^{\mathrm{U}}$, $S_{\mathrm{sf}}^{\mathrm{L}}$, $S_{\mathrm{sf}}^{\mathrm{O}}$, and $S_{\mathrm{sf}}^{\mathrm{Z}}$, which were determined arbitrarily. Under the above conditions, the trabecular remodeling simulation was performed by the workstation with 2 CPUs (Intel Xeon 5690) for about 3 hours.

3. Results

3.1. Changes in cancellous bone morphology

We applied the mathematical model of trabecular bone remodeling to simulate the remodeling of a cube of cancellous bone over a 30-day period in order to investigate the

mechanical adaptation to uniaxial or bending loads. Figs. 3 and 4 show the morphological changes in cancellous bone under uniaxial loading and bending loading, respectively. In both figures, the color indicates the 1-day average of the fluid-induced shear stress acting on the osteocyte processes, which is a driving force of bone remodeling. Independent of the type of external loading, the morphology of the cancellous bone gradually changed over time and the remodeled trabeculae had approximately circular cross-sections, as shown in Figs. 3d and 4d.

The application of a uniaxial load (Fig. 3) resulted in bone resorption on all cancellous bone surfaces for the first 3 days due to the low fluid-induced shear stress, leading to a decrease in the bone volume fraction. After this stage, bone formation began on the vertically oriented trabeculae exposed to greater fluid-induced shear stress, despite the preferential loss of the horizontal trabeculae. Successive remodeling gradually decreased the degree of trabecular connectivity, and the trabeculae in the cancellous bone reoriented parallel to the direction of loading by the end of the 30-day simulation.

The application of a bending load to cancellous bone produced significant bone erosion around the central region for analysis, which was close to the neutral axis of bending, in the first 3 days, as shown in Fig. 4. During the period from 3 days to 6 days, large numbers of trabeculae were lost from this region due to insufficient mechanical stimuli to osteocytes, while bone deposition occurred in the sides of the cancellous bone cube. After 30 days, the cancellous bone architecture reached a state of remodeling equilibrium in which the trabeculae around the central region were essentially absorbed and the remaining trabeculae aligned parallel to the direction of loading. This sequence of bone remodeling resulted in a

locally inhomogeneous trabecular pattern within the cancellous bone cube.

3.2. Distributions of mechanical quantities

The spatial distributions of the mechanical quantities of the trabeculae are important determinants of the cancellous bone morphology in the state of remodeling equilibrium. The previously proposed mathematical model for bone remodeling assumed several mechanical quantities to be mechanical stimuli regulating the remodeling process (Gerhard et al., 2009). To investigate the relationship between the cancellous bone architecture and the mechanical environment at the trabecular level, we focused on the distribution of von Mises equivalent stress σ_{eq} and SED U under the maximum load in 1 day as typical mechanical quantities. For the purpose of comparison, we introduced the deviation of both mechanical quantities defined as

$$\bar{Q} = Q - \mathrm{Mean}\left(Q\right), \tag{1}$$

where Q is either an equivalent stress, $Q = \sigma_{\mathrm{eq}}$, or a SED, $Q = U$. Mean(Q) denotes the mean value of Q in the cancellous bone included in the region for analysis.

The distributions of the volume fractions corresponding to the deviation of equivalent stress $\bar{\sigma}_{\mathrm{eq}}$ are shown in Fig. 5. Fig. 5a is for the case under uniaxial loading and Fig. 5b for the case under bending loading. The mean value and the standard deviation (s.d.) of the equivalent stress at different stages of remodeling are shown in Table 3 in the form: (mean ± s.d.). The initial distributions were asymmetric with respect to the mean value under both types of loading, although there was a little difference in their kurtosis values. Their

distributions shifted to nearly symmetrical bell-shaped curves as bone remodeling progressed. As shown in Table 3, the standard deviation of the equivalent stress decreased by 32% during the 30-day simulation regardless of the type of loading, while the mean value increased in both cases.

As for the deviation of SED $\bar{U}$, Figs. 6a and 6b show the distributions of the volume fractions under uniaxial loading and bending loading, respectively. The corresponding mean value and standard deviation of SED are listed in Table 4. The initial distribution curves under both types of loading have similar characteristics, e.g., strong asymmetry with respect to the mean value, sharp peaks, and fat tails in the positive direction. Adaptation of the bone to the external loading reduced the kurtosis and shifted the peak position toward the mean value. At the end of the 30-day remodeling simulation, the deviation of the peak position from the mean value was smaller under the bending load than under the uniaxial load. It must be noted that the standard deviation of SED increased by 47% under uniaxial loading but decreased by 43% under bending loading.

4. Discussion

The process by which the cancellous bone architecture adapts to the mechanical environment has a hierarchy from the microscopic cellular level to the macroscopic tissue level. The apparent changes in the density and orientation of cancellous bone result from bone remodeling on the surfaces of the individual trabeculae, and the changes in trabecular morphology are caused by the metabolic activities of numerous bone cells. In this study, we

represented this hierarchical regulatory process in a mathematical model and demonstrated the structural changes in cancellous bone during uniaxial or bending loading *in silico*. Previous simulation models of the adaptation of the trabecular microstructure have assumed that remodeling is driven by mechanical stimuli, such as stress and strain, at the trabecular level (e.g., Huiskes et al., 2000). In contrast to these models, our model considers the interstitial fluid flow, which acts directly on the osteocyte processes within the bone matrix, to be the most important stimulus. This simulation method should enable elucidation of the processes by which normal or pathological trabecular architecture develops in response to mechanical conditions at the cellular level.

The cancellous bone architecture formed by bone remodeling is significantly influenced by the rate of the applied load. In order to investigate its effects, we previously simulated a remodeling process of a single trabecula under cyclic loadings with various frequencies (Kameo et al., 2011). The results showed that the trabecular thickness increased due to large fluid-induced shear stress close to the surface with the increase in the loading frequency. The qualitatively same results would be expected for the remodeling simulation of cancellous bone cube. In the present simulation, we imposed monotonously increasing loads $\sigma = \sigma_3(x_1, x_2)t$ for 0.25 sec per day, as shown in Fig. 2, instead of cyclic loads to reduce the computational cost. By regulating the function $\sigma_3(x_1, x_2)$ and the loading time, it is possible to express the arbitrary loading rate.

The simulation results obtained herein indicated that subjecting cancellous bone with randomly arranged trabeculae to external loading resulted in alignment of the trabeculae

parallel to the direction of loading and a well-organized architecture specific to the type of external loading, as shown in Figs. 3 and 4. Such reorientation of the trabeculae is a reasonable phenomenon from the viewpoint of functional adaptation and agrees qualitatively with *in-vivo* experimental observations of cancellous bone architecture under controlled mechanical conditions (Goldstein et al., 1991; Guldberg et al., 1997a, b). Comparing the cancellous bone morphology in the remodeling equilibrium state between the 2 loading conditions, as shown in Figs. 3d and 4d, shows that the trabecular pattern is more inhomogeneous under bending loading due to loss of bone around the central region for analysis, which corresponds to the neutral axis of bending. Although *in-vivo* experimental studies have not yet succeeded in confirming this phenomenon, a trabecular remodeling simulation based on the phenomenological rule that remodeling progresses toward a locally uniform state of equivalent stress suggested a similar pattern (Tsubota and Adachi, 2005). Under all types of loading, the trabeculae in the remodeling equilibrium state had approximately circular cross-sections because cylindrical trabecular morphology uniformizes the interstitial fluid velocity. The characteristic cross-sectional shape agrees with the anatomical observations of cancellous bone and first represented by our original remodeling model. These results indicate that our mathematical model for trabecular bone remodeling can successfully predict the macroscopic changes in cancellous bone architecture from the microscopic cellular activities.

The distributions of the mechanical quantities at the trabecular level are generally non-uniform due to the complexity of cancellous bone architecture. Hence, the form of the

distribution function depends on the specific mechanical quantity (Tsubota and Adachi, 2006). Comparison of the distribution curves for equivalent stress and SED shown in Figs. 5 and 6 reveals that the distribution of SED is more sensitive to the small changes in cancellous bone morphology because SED is expressed as the quadratic form of stress or strain. Consequently, the standard deviation of the SED had increased under uniaxial loading but decreased under bending loading at the end of the 30-day simulation owing to its high sensitivity, as shown in Table 4, indicating that the uniformalization of the local SED may not be required for trabecular bone remodeling. On the other hand, the standard deviation of the equivalent stress decreased during the 30-day simulation under both types of loading. This suggests that our remodeling model with osteocytes as the mechanosensors can represent the phenomenological law of bone transformation toward a locally uniform state of stress or strain at the trabecular level.

The physical characteristics of our mathematical model is that bone remodeling is driven by the gradient of interstitial fluid pressure (see eq.(1) and (2)) instead of by the hydrostatic pressure itself. This means that the balance of bone resorption and formation is assumed to be regulated by the local differences in the mechanical conditions experienced by the trabeculae. In this sense, our model differs distinctly from the previous models in which remodeling was designed to obtain the global reference value of the particular mechanical quantity (Huiskes et al., 2000; McNamara and Prendergast, 2007) but is analogous to the model for remodeling caused by the local nonuniformity of equivalent stress (Adachi et al., 1997). As the latter model, despite its basis on the phenomenological rule, can successfully describe a

3-dimensional trabecular pattern similar to that in the actual human proximal femur (Tsubota et al., 2009), it seems reasonable to suppose that bone remodeling is influenced by the local distribution of certain mechanical quantities in the trabeculae rather than by the magnitude of stress or strain.

The proposed remodeling model contains 11 parameters to describe the 3 processes of trabecular bone remodeling without considering material properties of the trabecula (see Appendix): 5 parameters for (i) cellular mechanosensing (r_p, r_c, A_1, B_1, γ), 1 parameter for (ii) intercellular signal transmission (l_L), and 5 parameters for (iii) trabecular surface movement due to remodeling ($\dot{M}_{max}$, S_{sf}^{U}, S_{sf}^{L}, S_{sf}^{O}, S_{sf}^{Z}). Among these parameters, 5 parameters for cellular mechanosensing do not essentially influence the trabecular bone architecture because we assumed that they are constant by ignoring the position dependence of the geometry and dimensions of canaliculi. In the modeling of intercellular signal transmission, as the maximum distance for intercellular communication l_L increases, the mechanical state of trabeculae within more global area is reflected in the total stimulus on the trabecular surface S_{sf} and the bone volume fraction will increase due to the enlarged total stimulus. The maximum remodeling rate $\dot{M}_{max}$ is the parameter only governing the rate of bone resorption and formation, and has little influence on the trabecular bone architecture in the state of remodeling equilibrium. The role of the rest 4 parameters associated with the mechanical stimulus, S_{sf}^{U}, S_{sf}^{L}, S_{sf}^{O}, and S_{sf}^{Z}, has been discussed through a remodeling simulation for a single trabecula in Kameo et al. (2011), which reported that the morphological changes in the trabeculae are more sensitive to the parameter set of S_{sf}^{O} and S_{sf}^{Z} than to that of S_{sf}^{U} and

S_{sf}^{L}. These features are still valid in the present simulation.

In our mathematical model, complex 3-dimensional architectures of the lacuno-lanalicular porosity and the osteocyte network are ignored for simplicity even though they have a strong anisotropy. The effects of the microstructure on the osteocytic mechanotransduction via interstitial fluid flow can be represented in our simulation by using anisotropic permeability tensor in the poroelastic analysis and considering the orientation dependence of the volume fraction of the canaliculi $\rho_c(\boldsymbol{n})$ (Kameo et al., 2010). In addition, our mathematical model is limited by the assumption of an empirical relationship between the rate of trabecular surface remodeling $\dot{M}$ and the total stimulus on the trabecular surface S_{sf}, which can be regarded as an index of local fluid pressure gradient. The effectiveness of this conventionally used rate equation has been shown in previous remodeling simulations (e.g., McNamara and Prendergast, 2007), while recent experimental studies have cast doubt on the concept of a lazy zone at the tissue level (Sugiyama et al., 2012; Schulte et al., 2013). In order to predict the bone remodeling process more quantitatively, it will be essential to set the empirical parameters, S_{sf}^{U}, S_{sf}^{L}, S_{sf}^{O}, and S_{sf}^{Z}, appropriately with reference to relevant experimental findings.

While limited by the rate equation of trabecular surface remodeling, our mathematical model has the advantage of being able to investigate the effects of cellular mechanosensing and intercellular communication on the structural changes in cancellous bone. This trabecular remodeling simulation will definitely contribute to elucidating the mechanism of bone functional adaptation as a result of cellular activities. Future incorporation of the signaling

cascade of bone cells into the mathematical model will make our simulation model a powerful tool for such clinical applications as prediction of the effects of drugs targeting specific bone cells and the expected course of bone disease.

Acknowledgements

This study was partially supported by a Grant-in-Aid for Research Activity Start-up (23860044) and the Funding Program for Next Generation World-Leading Researchers (LR017) from the Japan Society for the Promotion of Science (JSPS).

Appendix

In the cellular mechanosensing process, osteocytes were assumed to be sensitive to fluid-induced shear stress on their cellular processes, and the biochemical signal produced by the stimulated osteocytes was assumed to be proportional to the shear force on the processes. Adopting the microstructure model of Weinbaum et al. (1994) for modeling the flow of interstitial fluid through a pericellular matrix in an annular canaliculus, and using the fluid pressure gradient at the trabecular level ∇p, the fluid-induced shear stress τ_{p} acting on the osteocyte processes aligned in direction $\boldsymbol{n}$ is given as

$$\tau_{\mathrm{p}}\left(\boldsymbol{x},\boldsymbol{n}\right)=\frac{qr_{\mathrm{p}}}{\gamma}\left[A_1 I_1\left(\frac{\gamma}{q}\right)-B_1 K_1\left(\frac{\gamma}{q}\right)\right]\nabla p\left(\boldsymbol{x}\right)\cdot\boldsymbol{n}\,, \tag{2}$$

where q is the ratio of the radius of the canaliculus r_{c} to that of the process r_{p}, i.e., $q=r_{\mathrm{c}}/r_{\mathrm{p}}$, and I_1 and K_1 are the modified Bessel functions of the first order. The coefficients A_1 and B_1 and the parameter γ are defined in Weinbaum et al. (1994).

As osteocytes are stimulated by the fluid-induced shear stress τ_p, the signal $S_{oc}(\boldsymbol{x})$ produced by the osteocytes per unit bone volume can be expressed, using the volume fraction of the canaliculi oriented in direction $\boldsymbol{n}$, $\rho_c(\boldsymbol{n})$, (Kameo et al., 2010), as

$$S_{oc}(\boldsymbol{x}) = \int_0^{2\pi} d\varphi \int_0^{\pi/2} \alpha \frac{2r_p}{r_c^2} \rho_c(\boldsymbol{n}) \left| \overline{\tau_p(\boldsymbol{x},\boldsymbol{n})} \right| \sin\theta d\theta, \tag{3}$$

where θ is the angle between the vector $\boldsymbol{n}$ and the x_3-axis in the arbitrary Cartesian coordinate system, φ is the angle between the x_1-axis and the projection of $\boldsymbol{n}$ onto the x_1x_2-plane measured counterclockwise, α is the mechanosensitivity of the osteocytes, and $\left|\overline{\tau_p(\boldsymbol{n})}\right|$ is the time-averaged shear stress over the course of 1 day. For simplicity, we ignored individual variability in osteocyte mechanosensitivity by setting $\alpha = 1$ and assumed the isotropy of canalicular orientation, i.e., $\rho_c(\boldsymbol{n}) = \phi/2\pi$, where ϕ is the porosity of the trabeculae.

The signals produced are modeled to be transmitted to the cells located on the trabecular surface, such as osteoclasts and osteoblasts, through the intercellular network. The surface cell is assumed to receive the signals from the osteocytes within a limited surrounding region Ω. With the use of a weight function $w(l)$ that represents the decay in the signal intensity relative to the distance l, the total stimulus S_{sf} on the trabecular surface position $\boldsymbol{x}_{sf}$ is obtained in the form

$$S_{sf}(\boldsymbol{x}_{sf}) = \int_\Omega w(l) S_{oc}(\boldsymbol{x}) d\Omega, \quad w(l) = 1 - l/l_L \ (l \le l_L), \tag{4}$$

where $l = |\boldsymbol{x}_{sf} - \boldsymbol{x}|$. Here, l_L denotes the maximum distance for intercellular communication.

To express the trabecular surface remodeling, we introduced the piecewise sinusoidal function that describes the relationship between the rate of trabecular surface remodeling $\dot{M}$ and the total stimulus on the trabecular surface S_{sf}, as shown in Fig. 1. This empirical function

indicates that bone resorption is initiated by stimuli below the remodeling equilibrium and bone formation is initiated by stimuli exceeding the equilibrium. In this function, S_{sf}^{U} is the upper threshold for bone formation, S_{sf}^{L} is the lower threshold for bone resorption, S_{sf}^{O} is a stimulus at the remodeling equilibrium, and S_{sf}^{Z} is the width of the lazy zone. The maximum rates of resorption and formation are assumed to have the same absolute value $\dot{M}_{max}$ to simplify the numerical algorithm, while the formation rate of osteoblasts is much smaller than the resorption rate of osteoclasts in reality. The level set method (Osher and Sethian, 1988), which is a numerical technique for tracking the interfaces and shapes of materials, was employed to express trabecular surface movement in this simulation.

References

Adachi, T., Aonuma, Y., Ito, S., Tanaka, M., Hojo, M., Takano-Yamamoto, T., Kamioka, H., 2009a. Osteocyte calcium signaling response to bone matrix deformation. J. Biomech. 42, 2507-2512.

Adachi, T., Aonuma, Y., Tanaka, M., Hojo, M., Takano-Yamamoto, T., Kamioka, H., 2009b. Calcium response in single osteocytes to locally applied mechanical stimulus: Differences in cell process and cell body. J. Biomech. 42, 1989-1995.

Adachi, T., Aonuma, Y., Taira, K., Hojo, M., Kamioka, H., 2009c. Asymmetric intercellular communication between bone cells: Propagation of the calcium signaling. Biochem. Biophys. Res. Commun. 389, 495-500.

Adachi, T., Kameo, Y., Hojo, M., 2010. Trabecular bone remodeling simulation considering osteocytic response to fluid-induced shear stress. Phil. Trans. R. Soc. A 368, 2669-2682.

Adachi, T., Tomita, Y., Sakaue, H., Tanaka, M., 1997. Simulation of trabecular surface remodeling based on local stress nonuniformity. JSME Int. J. 40C, 782-792.

Adachi, T., Tsubota, K., Tomita, Y., Hollister, S.J., 2001. Trabecular surface remodeling simulation for cancellous bone using microstructural voxel finite element models. J. Biomech. Eng. 123, 403-409.

Beno, T., Yoon, Y.J., Cowin, S.C., Fritton, S.P., 2006. Estimation of bone permeability using accurate microstructural measurements. J. Biomech. 39, 2378-2387.

Bonewald, L.F., Johnson, M.L., 2008. Osteocytes, mechanosensing and Wnt signaling. Bone 42, 606-615.

Burger, E.H., Klein-Nulend, J., 1999. Mechanotransduction in bone - Role of the lacuno-canalicular network. FASEB J. 13, S101-S112.

Cowin, S.C., 1999. Bone poroelasticity. J. Biomech. 32, 217-238.

Cowin, S.C., Moss-Salentijn, L., Moss, M.L., 1991. Candidates for the mechanosensory system in bone. J. Biomech. Eng. 113, 191-197.

Fritton, S.P., Weinbaum, S., 2009. Fluid and solute transport in bone: flow-induced mechanotransduction. Annu. Rev. Fluid Mech. 41, 347-374.

Gerhard, F.A., Webster, D.J., van Lenthe, G.H., Muller, R., 2009. In silico biology of bone modelling and remodelling: adaptation. Phil. Trans. R. Soc. A 367, 2011-2030.

Goldstein, S.A., Matthews, L.S., Kuhn, J.L., Hollister, S.J., 1991. Trabecular bone remodeling: An experimental model. J. Biomech. 24, 135-150.

Guldberg, R.E., Caldwell, N.J., Guo, W.E., Goulet, R.W., Hollister, S.J., Goldstein, S.A., 1997a. Mechanical stimulation of tissue repair in the hydraulic bone chamber. J. Bone Miner. Res. 12, 1295-1302.

Guldberg, R.E., Richards, M., Caldwell, N.J., Kuelske, C.L., Goldstein, S.A., 1997b. Trabecular bone adaptation to variations in porous-coated implant topology. J. Biomech. 30, 147-153.

Han, Y., Cowin, S.C., Schaffler, M.B., Weinbaum, S., 2004. Mechanotransduction and strain amplification in osteocyte cell processes and flow across the endothelial glycocalyx. Proc. Natl. Acad. Sci. U.S.A. 101, 16689-16694.

Huiskes, R., Weinans, H., Grootenboer, H.J., Dalstra, M., Fudala, B., Slooff, T.J., 1987. Adaptive bone-remodeling theory applied to prosthetic-design analysis. J. Biomech. 20, 1135-1150.

Huiskes, R., Ruimerman, R., Van Lenthe, G.H., Janssen, J.D., 2000. Effects of mechanical forces on maintenance and adaptation of form in trabecular bone. Nature 405, 704-706.

Huo, B., Lu, X.L., Hung, C.T., Costa, K.D., Xu, Q., Whitesides, G.M., Guo, X.E., 2008. Fluid flow induced calcium response in bone cell network. Cell. Mol. Bioeng. 1, 58-66.

Jang, I.G., Kim, I.Y., 2008. Computational study of Wolff's law with trabecular architecture in the human proximal femur using topology optimization. J. Biomech. 41, 2353-2361.

Jaworski, Z.F., Lok, E., 1972. The rate of osteoclastic bone erosion in haversian remodeling sites of adult dogs rib. Calcif. Tissue Res. 10, 103-112.

Kameo, Y., Adachi, T., Hojo, M., 2008. Transient response of fluid pressure in a poroelastic material under uniaxial cyclic loading. J. Mech. Phys. Solids 56, 1794-1805.

Kameo, Y., Adachi, T., Hojo, M., 2009. Fluid pressure response in poroelastic materials subjected to cyclic loading. J. Mech. Phys. Solids 57, 1815-1827.

Kameo, Y., Adachi, T., Hojo, M., 2010. Estimation of bone permeability considering the morphology of lacuno-canalicular porosity. J. Mech. Behav. Biomed. Mater. 3, 240-248.

Kameo, Y., Adachi, T., Hojo, M., 2011. Effects of loading frequency on the functional adaptation of trabeculae predicted by bone remodeling simulation. J. Mech. Behav. Biomed. Mater. 4, 900-908.

Kamioka, H., Kameo, Y., Imai, Y., Bakker, A.D., Bacabac, R.G., Yamada, N., Takaoka, A., Yamashiro, T., Adachi, T., Klein-Nulend, J., 2012. Microscale fluid flow analysis in human osteocyte canaliculus using a realistic high-resolution image-based three-dimensional model. Integr. Biol. 4, 1198-1206.

Kamioka, H., Honjo, T., Takano-Yamamoto T., 2001. A three-dimensional distribution of osteocyte processes revealed by the combination of confocal laser scanning microscopy and differential interface contrast microscopy. Bone 28, 145-149.

Kamioka, H., Murshid, S.A., Ishihara, Y., Kajimura, N., Hasegawa, T., Ando, R., Sugawara, Y., Yamashiro, T., Takaoka, A., Takano-Yamamoto T., 2009. A method for observing silver-stained osteocytes in situ in 3-μm sections using ultra-high voltage electron microscopy tomography. Microsc. Microanal. 15, 377-383.

Knothe Tate, M.L., Knothe, U., Niederer, P., 1998. Experimental elucidation of mechanical load-induced fluid flow and its potential role in bone metabolism and functional adaptation. Am. J. Med. Sci. 316, 189-195.

McNamara, L.M., Prendergast, P.J., 2007. Bone remodelling algorithms incorporating both strain and microdamage stimuli. J. Biomech. 40, 1381-1391.

Mullender, M.G., Huiskes, R., 1995. Proposal for the regulatory mechanism of Wolff’s law. J.

Orthop. Res. 13, 503-512.

Mullender, M.G., Huiskes, R., Weinans, H., 1994. A physiological approach to the simulation of bone remodeling as a self-organizational control process. J. Biomech. 27, 1389-1394.

Mulvihill, B.M., Prendergast, P.J., 2008. An algorithm for bone mechanoresponsiveness: implementation to study the effect of patient-specific cell mechanosensitivity on trabecular bone loss. Comput. Methods Biomech. Biomed. Eng. 11, 443-451.

Nakashima, T., Hayashi, M., Fukunaga, T., Kurata, K., Oh-hora, M., Feng, J.Q., Bonewald, L.F., Kodama, T., Wutz, A., Wagner, E.F., Penninger, J.M., Takayanagi, H., 2011. Evidence for osteocyte regulation of bone homeostasis through RANKL expression. Nat. Med. 17, 231-1234.

Osher, S., Sethian, J.A., 1988. Fronts propagating with curvature-dependent speed: algorithms based on Hamilton-Jacobi formulation. J. Comput. Phys. 79, 12-49.

Parfitt, A.M., 1994. Osteonal and hemi-osteonal remodeling: The spatial and temporal framework for signal traffic in adult human bone. J. Cell. Biochem. 55, 273-286.

Prendergast, P.J., Taylor, D., 1994. Prediction of bone adaptation using damage accumulation. J. Biomech. 27, 1067-1076.

Ruimerman, R., Hilbers, P., van Rietbergen, B., Huiskes, R., 2005. A theoretical framework for strain-related trabecular bone maintenance and adaptation. J. Biomech. 38, 931-941.

Schulte, F.A., Ruffoni, D., Lambers, F.M., Christen, D., Webster D.J., Kuhn, G., Muller, R., 2013. Local mechanical stimuli regulate bone formation and resorption in mice at the tissue level. Pros One 8, e62172.

Smit, T.H., Huyghe, J.M., Cowin, S.C., 2002. Estimation of the poroelastic parameters of cortical bone. J. Biomech. 35, 829-835.

Sugawara, Y., Kamioka, H., Honjo, T., Tezuka, K., Takano-Yamamoto, T., 2005. Three-dimensional reconstruction of chick calvarial osteocytes and their cell processes using confocal microscopy. Bone 36, 877-883.

Sugiyama, T., Meakin, L.B., Browne, W.J., Galea, G.L., Price, J.S., Lanyon, L.E., 2012. Bones' adaptive response to mechanical loading is essentially linear between the low strains associated with disuse and the high strains associated with the lamellar/woven bone transition. J. Bone Miner. Res. 27, 1784-1793.

Tatsumi, S., Ishii, K., Amizuka, N., Li, M.Q., Kobayashi, T., Kohno, K., Ito, M., Takeshita, S., Ikeda, K., 2007. Targeted ablation of osteocytes induces osteoporosis with defective mechanotransduction. Cell Metab. 5, 464-475.

Tsubota, K., Adachi, T., 2004. Change in the fabric and compliance tensors of cancellous bone due to trabecular surface remodeling, predicted by a digital image-based model. Comput. Methods Biomech. Biomed. Eng. 7, 187-192.

Tsubota, K., Adachi, T., 2005. Spatial and temporal regulation of cancellous bone structure: Characterization of a rate equation of trabecular surface remodeling. Med. Eng. Phys. 27, 305-311.

Tsubota, K., Adachi, T., 2006. Computer simulation study on local and integral mechanical quantities at single trabecular level as candidates of remodeling stimuli. J. Biomech. Sci. Eng. 1, 124-135.

Tsubota, K., Adachi, T., Tomita, Y., 2002. Functional adaptation of cancellous bone in human proximal femur predicted by trabecular surface remodeling simulation toward uniform stress state. J. Biomech. 35, 1541-1551.

Tsubota, K., Suzuki, Y., Yamada, T., Hojo, M., Makinouchi, A., Adachi, T., 2009. Computer simulation of trablecular remodeling in human proximal femur using large-scale voxel FE models: Approach to understanding Wolff's law. J. Biomech. 42, 1088-1094.

Wang, Y., McNamara, L.M., Schaffler, M.B., Weinbaum, S., 2007. A model for the role of integrins in flow induced mechanotransduction in osteocytes. Proc. Natl. Acad. Sci. U.S.A. 104, 15941-15946.

Weinbaum, S., Cowin, S.C., Zeng, Y., 1994. A model for the excitation of osteocytes by mechanical loading-induced bone fluid shear stresses. J. Biomech. 27, 339-360.

Wolff, J., 1892. Das gesetz der transformation der knochen. Hirschwald, Berlin.

Wolff, J., 1986. The law of bone remodeling. Springer, Berlin (translated by P. Maquet and R. Furlong).

You, L.D., Cowin, S.C., Schaffler, M.B., Weinbaum, S., 2001. A model for strain amplification in the actin cytoskeleton of osteocytes due to fluid drag on pericellular matrix. J. Biomech. 34, 1375-1386.

You, L.D., Weinbaum, S., Cowin S.C., Schaffler M.B., 2004. Ultrastructure of the osteocyte process and its pericellular matrix. Anat. Rec. A 278A, 505-513.

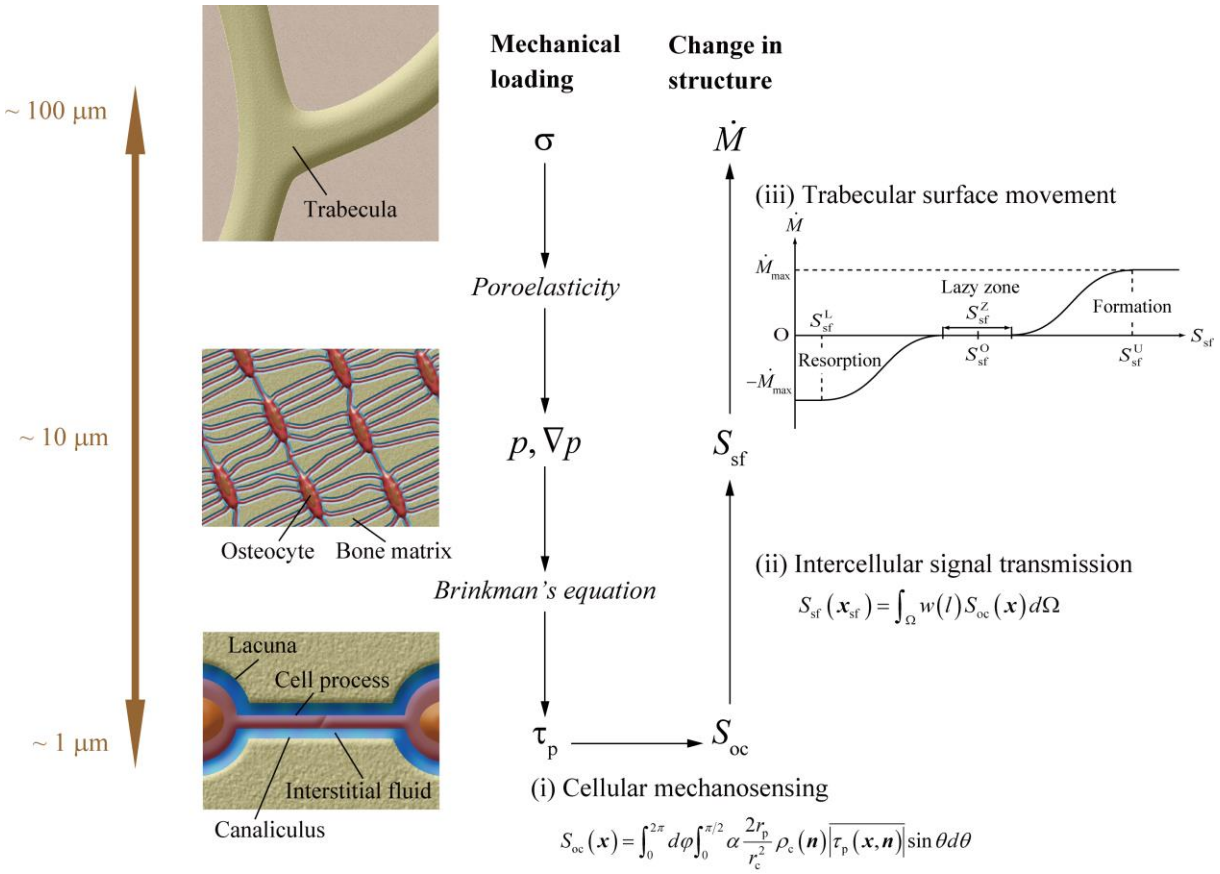

Fig. 1 Theoretical framework for trabecular bone remodeling considering the mechanical hierarchy from the microscopic level (~ 1 μm) to the macroscopic level (~ 100 μm). The bone remodeling process consists of the following 3 parts: (i) cellular mechanosensing, (ii) intercellular signal transmission, and (iii) trabecular surface movement.

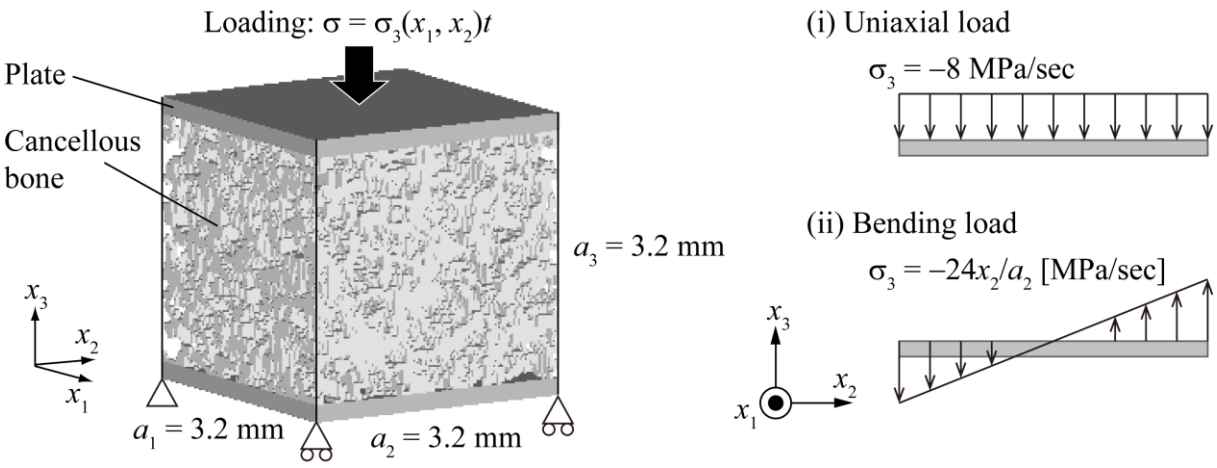

Fig. 2 A 3-dimensional model of cancellous bone for simulation of trabecular remodeling. In the initial configuration, all of the trabeculae are randomly oriented. This model was subjected to 2 types of monotonously increasing loading through the upper plate, (i) uniaxial loading and (ii) bending loading.

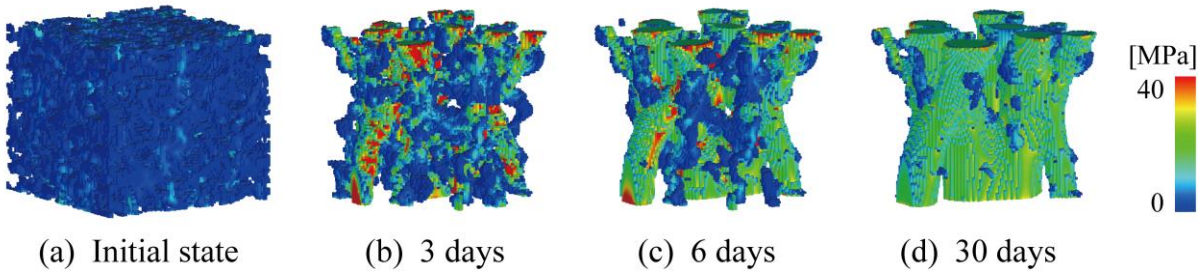

Fig. 3 Changes in the cancellous bone morphology and average fluid-induced shear stresses in 1 day $\overline{|\tau_p|}$ under uniaxial loading.

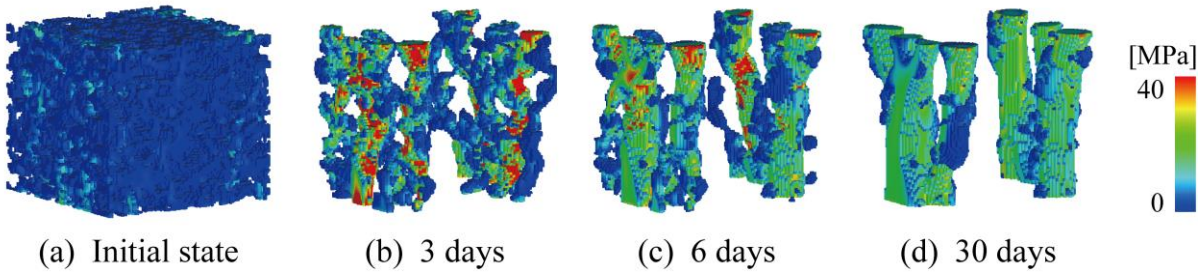

Fig. 4 Changes in the cancellous bone morphology and average fluid-induced shear stresses in 1 day $\overline{|\tau_p|}$ under bending loading.

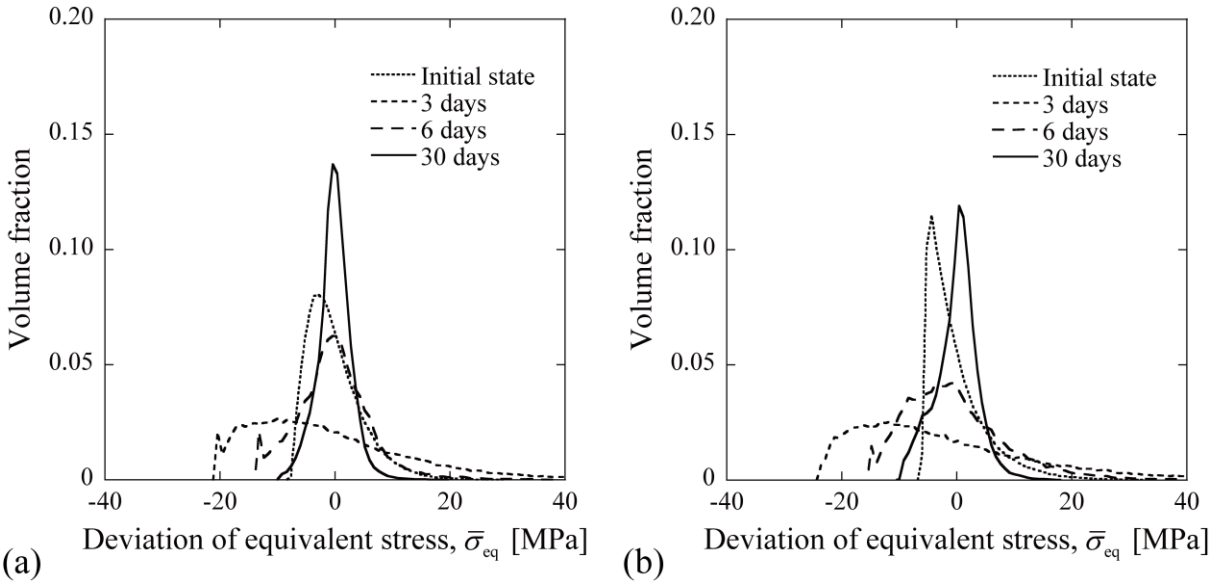

Fig. 5 Distributions of the volume fraction corresponding to the deviation of equivalent stress $\bar{\sigma}_{eq}$: (a) under uniaxial loading and (b) under bending loading.

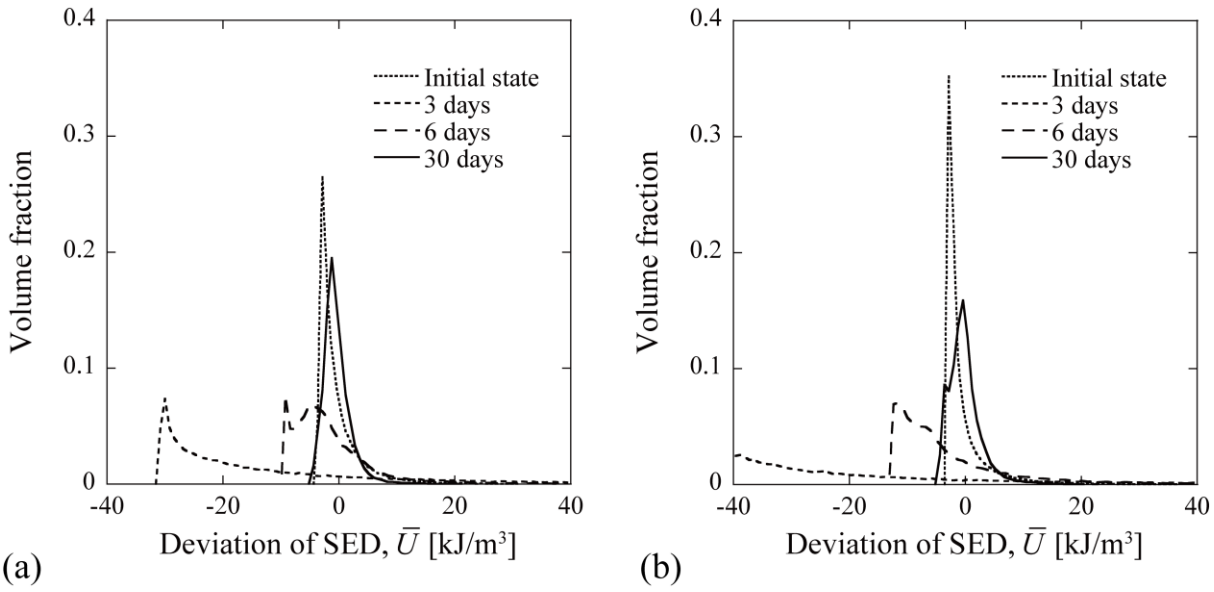

Fig. 6 Distributions of the volume fraction corresponding to the deviation of strain energy density (SED) $\bar{U}$: (a) under uniaxial loading and (b) under bending loading.

Table 1 Material properties of the trabecula as a poroelastic material (Smit et al., 2002; Beno et al., 2006).

Symbol (unit)	Description	Value
k (m^2)	Intrinsic permeability	1.1×10^{-21}
μ (Pa·s)	Fluid viscosity	1.0×10^{-3}
G (GPa)	Shear modulus	5.94
ν	Drained Poissons's ratio	0.325
K_s (GPa)	Solid bulk modulus	17.66
K_f (GPa)	Fluid bulk modulus	2.3
ϕ	Porosity	0.05

Permeability was estimated by the method of Beno et al. (2006).
The other constants were taken from Smit et al. (2002).

Table 2 Parameter settings for the trabecular remodeling simulation (Jaworski and Lok, 1972; You et al., 2004; Huo et al., 2008; Adachi et al., 2009c).

Symbol (unit)	Description	Value
r_p (nm)	Radius of osteocyte process	52[a]
r_c (nm)	Radius of canaliculus	129.5[a]
l_L (μm)	Maximum distance for intercellular communication	200[b,c]
$\dot{M}_{max}$ (μm/day)	Maximum remodeling rate	40[d]
S_{sf}^{U} (μN)	Upper threshold for bone formation	1.0
S_{sf}^{L} (μN)	Lower threshold for bone resorption	13
S_{sf}^{O} (μN)	Stimulus at remodeling equilibrium	7.0
S_{sf}^{Z} (μN)	Width of lazy zone	10

[a] You et al. (2004)
[b] Huo et al. (2008)
[c] Adachi et al. (2009c)
[d] Jaworski and Lok (1972)

Table 3 Mean value and standard deviation (s.d.) of von Mises equivalent stress during remodeling.

	von Mises equivalent stress, σ_{eq} [MPa]	
	Uniaxial load	Bending load
Initial state	7.24 ± 4.93	5.89 ± 5.46
3 days	20.4 ± 16.9	24.0 ± 20.7
6 days	13.1 ± 7.15	14.5 ± 9.62
30 days	9.80 ± 3.36	9.94 ± 3.72

(mean ± s.d.)

Table 4 Mean value and standard deviation (s.d.) of the strain energy density (SED) during remodeling.

	SED, U [kJ/m^3]	
	Uniaxial load	Bending load
Initial state	3.30 ± 4.92	2.77 ± 6.05
3 days	30.6 ± 78.4	44.4 ± 130
6 days	9.43 ± 15.5	12.5 ± 23.7
30 days	4.35 ± 7.25	4.19 ± 3.46

(mean ± s.d.)